MONTANA STATE UNIVERSITY LIBRARY

The impacts of mountain pine beetle disturbance on the energy balance of snow during the melt period

Authors: Christopher M. Welch, Paul Stoy, F. Aaron Rains, Aiden V. Johnson, and Brian L. McGlynn

This is the peer reviewed version of the following article: see full citation below, which has been published in Hydrological Processes and can be found in final form at http://dx.doi.org/10.1002/hyp.10638. This article may be used for non-commercial purposes in accordance with Wiley Terms and Conditions for Self-Archiving.

Welch, Christopher M., Paul Stoy, F. Aaron Rains, Aiden V. Johnson, and Brian L. McGlynn. "The impacts of mountain pine beetle disturbance on the energy balance of snow during the melt period." Hydrological Processes 30, no. 4 (2015): 588-602

Made available through Montana State University's ScholarWorks
scholarworks.montana.edu

The impacts of mountain pine beetle disturbance on the energy balance of snow during the melt period

Christopher M. Welch,[1] Paul C. Stoy,[1]* F. Aaron Rains,[1] Aiden V. Johnson[1] and Brian L. McGlynn[2]

[1] *Department of Land Resources and Environmental Sciences, Montana State University, Bozeman, MT, 59717, USA*
[2] *Division of Earth and Ocean Sciences, Nicholas School of the Environment, Duke University, Durham, NC, 27708, USA*

Abstract:

Mountain snowpacks provide most of the annual discharge of western US rivers, but the future of water resources in the western USA is tenuous, as climatic changes have resulted in earlier spring melts that have exacerbated summer droughts. Compounding changes to the physical environment are biotic disturbances including that of the mountain pine beetle (MPB), which has decimated millions of acres of western North American forests. At the watershed scale, MPB disturbance increases the peak hydrograph, and at the stand scale, the 'grey' phase of MPB canopy disturbance decreases canopy snow interception, increases snow albedo, increases net shortwave radiation, and decreases net longwave radiation *versus* the 'red' phase. Fewer studies have been conducted on the red phase of MPB disturbance and in the mixed coniferous stands that may follow MPB-damaged forests. We measured the energy balance of four snowpacks representing different stages of MPB damage, management, and recovery: a lodgepole pine stand, an MPB-infested stand in the red phase, a mixed coniferous stand (representing one successional trajectory), and a clear-cut (representing reactive management) in the Tenderfoot Creek Experimental Forest in Montana, USA. Net longwave radiation was lower in the MPB-infested stand despite higher basal area and plant area index of the other forests, suggesting that the desiccated needles serve as a less effective thermal buffer against longwave radiative losses. Eddy covariance observations of sensible and latent heat flux indicate that they are of similar but opposite magnitude, on the order of 20 MJ m^{-2} during the melt period. Further analyses reveal that net turbulent energy fluxes were near zero because of the temperature and atmospheric vapour pressure encountered during the melt period. Future research should place snow science in the context of forest succession and management and address important uncertainties regarding the timing and magnitude of needlefall events. Copyright © 2015 John Wiley & Sons, Ltd.

INTRODUCTION

Mountain snowpacks provide up to 75% of the annual discharge of major rivers in the western USA (Palmer, 1988; Cayan, 1996), but the sustainability of this resource is uncertain as climatic changes have resulted in earlier spring melts that have exacerbated summer droughts (Westerling *et al*., 2006; Hamlet *et al*., 2007). Peak run-off in the western USA is predicted to occur 1 month earlier over the course of the next century, and less water will likely be available in late summer and fall when water scarcity is most prevalent (Barnett *et al*., 2005). Meanwhile, extreme winter precipitation events are likely to increase in intensity (Dominguez *et al*., 2012). An improved mechanistic understanding of snow accumulation and ablation is critical for forecasting the future of water resources in the West.

Associated with physical changes to climate are alterations to the biological environment via the massive outbreak of the mountain pine beetle (*Dendroctonus ponderosae* Hopkins, hereafter 'MPB') and other herbivores that have devastated several million hectares in western North America (Raffa *et al*., 2008) leaving in their wake a forest, and a snowpack, transformed. MPB infestation has reached higher altitudes in response to climate change (Logan and Powell, 2001; Jessie *et al*., 2003; Aukema *et al*., 2008) with evidence of a shift from univoltine to multivoltine breeding cycles (Mitton and Ferrenberg, 2012). The large-scale encroachment of the MPB into the so-called 'watertower of the West' – the forests associated with the mountain snowpack – is cause for concern for water scientists and managers.

Stand-scale studies have increasingly focused on the mechanisms underlying snow accumulation and ablation across MPB disturbance sequences (Perrot *et al*., 2014).

Accumulation and ablation from forest snowpacks are controlled in part by wind scouring, solar radiation flux, and snow interception, all of which are closely tied to the forest canopy structure that the MPB alters (Harestad and Bunnell, 1981). Varhola *et al*. (2010) synthesized the results of 33 studies and found that 57% (72%) of the variance of relative changes in snowpack accumulation (ablation) was explained by changes in forest cover. A decrease in canopy cover is linked to an increase in snow accumulation as less canopy-intercepted snow is sublimated (Pomeroy *et al*., 2002; Varhola *et al*., 2010), noting that snowpack sublimation is enhanced in MPB killed stands (Biederman *et al*., 2014). Molotch *et al*. (2009), for example, reported a 29% increase in snow accumulation in open *versus* under-canopy sites and a faster rate of snowmelt with an increase in direct solar radiation load. MPB-infected watersheds as a consequence tend to produce increases in annual water yields with an advanced hydrograph (Potts, 1984; Bearup *et al*., 2014), i.e. a hydrograph that peaks earlier.

Recent studies on the impacts of MPB disturbance on snow processes found increased snow accumulation and ablation rates in infested stands (Boon, 2009; Pugh and Small, 2012; Pugh and Gordon, 2013). In combination, the response of snow accumulation and ablation to MPB damage can be understood using a conceptual model (Mikkelson *et al*., 2013; Pugh and Gordon, 2013): A dying canopy will accumulate less snow, absorb less incident shortwave radiation, absorb less momentum from the atmosphere with a corresponding increase in subcanopy wind speeds and hence sublimation (Pomeroy and Essery, 1999), and serve as a less effective thermal buffer against longwave radiation loss than an uninfested canopy, all else being equal. Combined with enhanced litterfall from dying canopies that decreases snow albedo (Winkler *et al*., 2010, 2014; Pugh and Small, 2012), snowpacks in MPB-impacted forests are likely to accumulate a greater amount of snow that melts faster. The importance of MPB-related changes to the canopy and snow, especially during the red phase, on the snow energy balance during the ablation period remains less frequently studied. No studies to date have continuously measured the energy balance of snow, including the turbulent exchange of sensible and latent heat flux between snow and atmosphere, in healthy and red-stage infested stands, and the clear-cut and mixed forests that may follow MPB infestation across the entire melt period.

We measured the energy balance of snow during the peak ablation period in a forest undergoing MPB attack, nearby mixed coniferous and lodgepole pine-dominated (*Pinus contorta* Dougl.) healthy stands, and a clear-cut. Our objectives are to improve understanding of the early stages of MPB infestation on snow ablation and to quantify how energy inputs into mountain snowpacks change across space-for-time succession and management chronosequences. The study was designed to capture end members in a sequence that begins with lodgepole pine, proceeds through MPB infestation, and results in either reactive management (clear-cut) or a subsequent increase in stand diversity (Stone and Wolfe, 1996), noting that other management and successional trajectories – including those related to fire (Lynch *et al*., 2006; Burles and Boon, 2011) – are also likely. We measured incident and outgoing shortwave and longwave radiation over the course of the melt period and uniquely use a subcanopy eddy covariance system in the lodgepole-dominated stand to measure sensible and latent heat flux between the snow surface and atmosphere for the purpose of exploring the contribution of these understudied terms to the snowpack energy balance. We finish with a prospectus for future studies of snowmelt that focuses on the community ecology of forest stands.

METHODS

Snow energy balance

The energy available to melt snow, Q_m, excluding lateral advective energy fluxes that we assume to be negligible (Marks and Dozier, 1992), can be written:

$$Q_m = R_{net} + H + \lambda E + G. \tag{1}$$

where H is the sensible heat flux, λE is the latent heat flux, and G is the soil heat flux. The net radiation (R_{net}) can also be written as a function of incident ($_{in}$) and outgoing ($_{out}$) or net ($_{net}$) shortwave (SW) and longwave (LW) components:

$$\begin{aligned} R_{net} &= SW_{in} - SW_{out} + LW_{in} - LW_{out} \\ &= SW_{net} + LW_{net} \end{aligned} \tag{2}$$

We measured all terms of Equation (1) – including H and λE using eddy covariance – at a lodgepole pine forest in the Tenderfoot Creek Experimental Forest (TCEF) in west-central Montana. We additionally measured all terms of Equation (2) at MPB-infested, mixed coniferous, and clear-cut ecosystems in TCEF, describing physical differences in the snow energy balance along a disturbance chronosequence (Figure 1).

Tenderfoot Creek Experimental Forest

TCEF is part of the United States Forest Service's Lewis and Clark National Forest and encompasses seven gauged watersheds within a 3693-ha area that make up the headwaters of Tenderfoot Creek. Elevation ranges from 1840 to 2421 m above sea level (a.s.l.) (Figure 1)

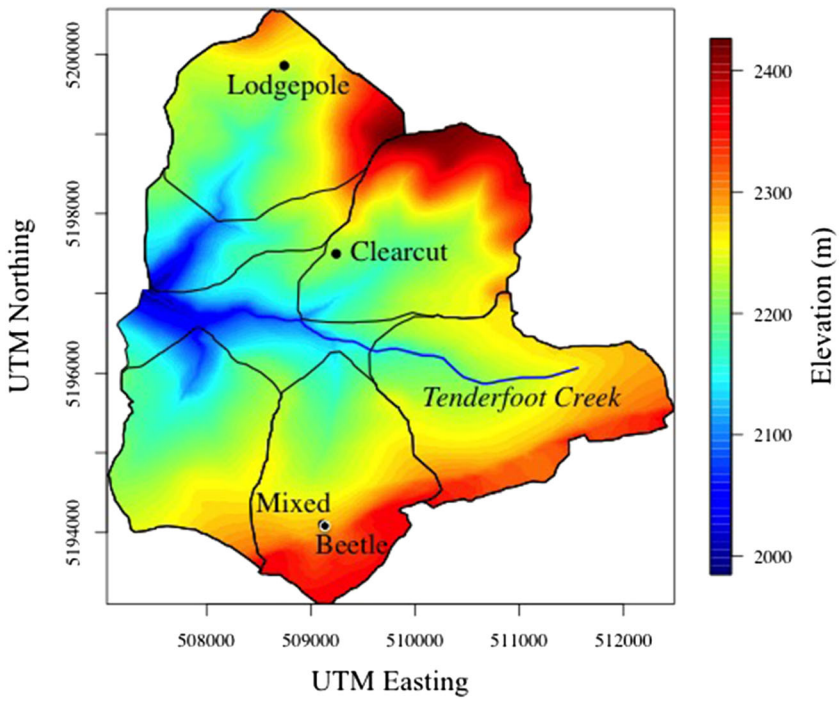


Figure 1. A map of the Tenderfoot Creek Experimental Forest, Montana, USA, with study locations UTM stands for the Universal Transverse Mercator coordinate system

with a mean of 2205 m (Pacific *et al*., 2011). Lodgepole pine makes up a large majority of the forest canopy, either as monotypic stands or in mixed coniferous forests with Engelmann spruce (*Picea engelmannii* Parry × Engelm.), whitebark pine (*Pinus albicaulis* Engelm.), and subalpine fir [*Abies lasiocarpa* (Hooker) Nutall]. Many areas of TCEF have low species and age-class diversity with forest communities dominated by even-aged lodgepole pine (Mincemoyer and Birdsall, 2006).

Climate conditions are temperate continental with an average annual precipitation of 880 mm that ranges from 594 to 1050 mm at the lowest and highest elevations (Jencso and McGlynn, 2011). About 70% of the precipitation at TCEF occurs between the months of November and May, primarily as snow (Farnes *et al*., 1995; Riveros-Iregui *et al*., 2011). Approximately 550 mm is lost to evapotranspiration and the mean annual run-off of Upper Tenderfoot Creek is ~300 mm (Pacific *et al*., 2010).

Unlike the characteristic MPB attacks found in British Columbia and other parts of the Rocky Mountains in which large tracks of homogeneous stands are infested (Kurz *et al*., 2008), the recent MPB infestation in TCEF has remained small and intermittent. Kaiser *et al*. (2012) used a three-component mixing model applied to Quickbird observations in combination with light detection and ranging data and found that approximately 2% of vegetation above 3 m in height at TCEF were in the red stage of disturbance as of 2010.

Lodgepole pine site

The lodgepole pine site is within the heavily instrumented 300-ha Stringer Creek subcatchment at TCEF (Emanuel *et al*., 2010). Since 2005, above-canopy meteorological and eddy covariance measurements have been made in a lodgepole pine-dominated forest at 30 m above the ground surface on a 40-m tower located at N46.9522479 W110.885312 (Riveros-Iregui and McGlynn, 2009; Emanuel *et al*., 2010, 2011; Riveros-Iregui *et al*., 2012; Mitchell *et al*., 2015). In the fall of 2010, a 3-m subcanopy tower was installed 19 m SSE of the tall tower at N46.95218 W110.88507 at an elevation of 2250 m a.s.l. The tower included a full suite of sensors for micrometeorological and energy balance measurements (Table I). A Campbell Scientific SR50A-L sonic depth sensor located at 1.75 m above the ground surface measured snow depth. Solar and thermal radiation data were measured at 2.13 m above the ground surface using an NR01 four-component net radiometer with expected daily average accuracy within 10% and a typical sensitivity range of 10–40 $\mu V\,W^{-1}\,m^{-2}$ (Hukseflux, Delft, The Netherlands). Air temperature and humidity were measured using a HMP45C (Vaisala, Helsinki, Finland) at 2.18 m. Snow surface temperature (T_{ss}) was measured using an SI-111 (Apogee Instruments, Logan, UT, USA). For ground heat flux (G), a self-calibrating HFP01 heat flux plate (Hukseflux) was buried 5 cm below the soil surface. G under snow is often assumed to be 3.13 $W\,m^{-2}$ in the absence of measurements

Table I. Micrometeorological measured at each site indicated with sensor description

Measurement	Sensor	Site
Incident and outgoing shortwave and longwave radiation	NR01 net radiometer[a]	All
Snow depth	SR50 sonic distance sensor	All
Snow temperature	Type T thermocouples	L, M, B
Snow surface temperature (T_{ss})[b]	SI-111 infrared temperature sensor	L, C
Air temperature (T_a)	HMP45C probe	L, C[c], M
Soil heat flux (G)	HFP01 Heat Flux Plate	L, C
Sensible heat flux (H)	CSAT3 and LI-7200	L
Latent heat flux (λE)	CSAT3 and LI-7200	L

L, lodgepole pine; C, clear-cut; M, mixed coniferous forest; B, beetle-infested mixed coniferous forest.
[a] A CRN1 net radiometer was installed in the clear-cut site.
[b] Snow surface temperature was measured using outgoing longwave radiation measurements from the NR01 net radiometer at the healthy and beetle-infested sites.
[c] T_a at the clear-cut site was measured using a shielded Type T thermocouple.

(Maidment, 1992; Boon, 2009), and we use G measurements here and at the clear-cut site to test these assumptions. Measurements were made every minute, and half-hour averages were logged using CR3000 and CR1000 data loggers (Campbell Scientific).

Sensible heat exchange (H) was measured using a CSAT-3 sonic anemometer (Campbell Scientific), and latent heat exchange (λE) was measured using the eddy covariance technique by coupling the sonic anemometer with an enclosed LI-7200 CO_2/H_2O infrared gas analyser (LiCor Inc., Lincoln, NE, USA), both at 2 m above the ground surface. Measurements were collected at 10 Hz, stored on the CR3000 data logger, and processed into half-hourly flux sums as described by Rains (2013). Data were filtered for periods of insufficient turbulence using a friction velocity (u*) threshold of 0.05 m s^{-1} identified by Rains (2013), broadly consistent with the median u* threshold identified by Misson *et al.* (2007), 0.06 m s^{-1}, across multiple subcanopy eddy covariance towers. We adopt the convention that energy fluxes into the snowpack are considered positive; this convention is the opposite of the typical micrometeorological convention that energy inputs to the atmosphere are considered positive. Missing data were infrequent and were gapfilled using linear relationships with R_{net} as described in Appendix A and Stoy *et al.* (2006).

Mountain pine beetle-infested and mixed coniferous sites

All terms of Equation (2) were measured at a stand in the red stage of MPB infestation at N46.900327 W110.880167 and at a nearby mixed coniferous stand 14 m to the NW at N46.900406 W110.880334, both at 2289 m a.s.l.

At the MPB-infested site, a NR01 radiometer and a SR50A distance sensor were installed at 1.75 m on a small tower. Five copper-constantan thermocouples mounted at 0, 25, 50, 75, and 100 cm above the ground were controlled by AM16/32B multiplexer (Campbell Scientific). All measurements were recorded at 5-min intervals, which were averaged every 30 min and logged by a CR1000 datalogger.

The tower in the mixed coniferous site included all instrumentation found at the infested stand positioned within 5 cm with respect to the ground surface of sensors at the MPB-infested stand (Table I). The mixed coniferous site was enhanced with an HMP45C temperature relative humidity sensor and a larger snow temperature ladder consisting of a free-standing 1.5-in. polyvinyl chloride pipe with five copper-constantan thermocouples positioned from ground level to 200 cm above the ground at 25-cm increments connected to an AM 16/32 multiplexer (Campbell Scientific). Five-minute observations were logged by a CR1000 and averaged hourly.

Clear-cut site

From 1999 to 2001, tree-thinning experiments were conducted to investigate the effects of different silvicultural treatments on water yield and sediment transport in TCEF (Woods *et al.*, 2006). In the Spring Park subcatchment, approximately 50% of the basal area was removed to create a mosaic of clear-cut and uncut lodgepole pine forest (Nippgen *et al.*, 2011). A 3-m tower was installed in a clear-cut section within Spring Park at N46.930957 W110.87856 and 2221 m a.s.l. by the Montana State University Watershed Hydrology Lab, including a CNR-1 four-component net radiometer at 2 m above the ground surface (Table I). In the fall of 2010, an SR50A-L sonic distance sensor was added 1.65 m above the ground surface to record snow depth, and an SI-111 was installed at the same height to measure T_{ss}. A HFP01 ground heat flux plate was installed 5 cm below the soil surface to measure G. Ten copper-constantan thermocouples were installed at multiple locations above and below

the soil surface and controlled by an AMT 25 multiplexer (Campbell Scientific). Measurements were recorded every minute, averaged over 30-min intervals, and were logged by a CR3000.

Forest measurements

Height and diameter at breast height were measured for all trees above breast height within 10 m of the respective tower in the subcanopy, infested, and healthy stands using a PM-5/1520 Height Meter (Suunto Oy, Vantaa, Finland) and Original Loggers Tape (Spencer Products, Twinsburg, OH, USA) (Table II). Plant area index (PAI) was estimated using a Beer's law exponential canopy radiation extinction model

$$PAI = \frac{\ln(\tau)}{-\sqrt{\alpha K \Omega}} \tag{3}$$

where leaf absorbtivity to shortwave radiation, α, is assumed to be 0.5 (Campbell and Norman, 1998), the leaf clumping factor Ω is assumed to be 0.6 (Stoy *et al*., 2006), and we assume an ellipsoidal leaf distribution for the extinction coefficient K (Campbell and Norman, 1998) with horizontal to vertical canopy projected area to equal 1.64 following Luo *et al*. (2001).

Snow water equivalent

A continuous estimate of snow water equivalent (SWE) is desirable to estimate Q_m for an analysis of the lodgepole pine site eddy covariance energy balance, which is rarely closed (Wilson *et al*., 2002; Leuning *et al*., 2012; Stoy *et al*., 2013). SWE was measured approximately monthly during the snow-covered period of both 2011 and 2012 using snow pits as described by Rains (2013) and/or a federal Sierra Snow Tube. Depth and weight of each core were recorded, with cores showing greater than 30% change in length to depth rejected. In some cases, 30% ratios of depth to core length were not achievable because of snow conditions such as depth hoar and were noted. If soil or vegetation was present at the bottom of the core, the volume of the impurity was subtracted from the total core length and discarded before weighing.

An estimate of SWE at the native half-hourly increment of the eddy covariance measurements is desirable for an analysis of the energy balance closure. We created linear models of SWE using hourly SWE observations from the Onion Park and Stringer Creek SNOpack TELemetry sites and manual SWE observations. Onion Park is at an elevation of 2258 m a.s.l. ~3 km from the MPB-infested and mixed-canopy sites and includes two SWE observations from relatively open (hereafter 'Onion I') and closed ('Onion II') canopy sites. Stringer Creek is 1996 m a.s.l. near the centre of TCEF less than 1 km from the clear-cut site (Figure 1). We selected the model with the minimum Akaike information criterion and Bayesian information criterion calculated using R (R Core Team, 2014) to obtain an hourly estimate of SWE at the lodgepole pine site and used linear interpolation to estimate SWE at the lodgepole pine site at half-hourly intervals.

The temporal change in SWE (*dSWE*) has units of water depth/time. The modelled energy flux associated with snowmelt, $Q_{m,m}$, is a function of dSWE:

$$Q_{m,m} = \lambda_f \rho_w dSWE \tag{4}$$

where λ_f is the latent heat of fusion (334 000 J kg^{-1}, noting that the latent heat of vapourization, λ, is implied

Table II. Stand characteristics at the lodgepole pine ('Lodgepole'), mountain pine beetle-infested ('Beetle'), and mixed coniferous ('Mixed') forests

Stand characteristic	Lodgepole	Beetle	Mixed
Mean DBH (cm)	26	27	18
DBH standard deviation (cm)	4.9	8.0	7.3
Basal area (m^2)[a]	1.2	2.3	1.8
Mean stand height (m)	16	20	22
Plant area index (m^2 m^{-2})	4.1	5.3	5.5
% Dead trees	0	54	24
% MPB-infected trees	0[b]	39	0
% Lodgepole pine	>96	76	63
Number of stems within a 10-m radius of the tower	23	41	71
Slope	8%	15%	15%
Aspect	SSE	NNW	NNW

The clear-cut site has a slope of 3% and a SSW aspect. DBH, diameter breast height; MPB, mountain pine beetle.
[a] Basal area is calculated for the area within a 10-m radius surrounding the respective tower.
[b] The lodgepole pine forest was in the nascent stages of MPB attack, but no trees within the 10-m radius surrounding the measurement tower were observed to be in the red phase during the study period.

in the definition of latent heat flux, λE) and ρ_w is the density of water (1000 kg m^{-3}).

Corrections for local slope

Radiometers were mounted in a level position, but the underlying snow followed topography at each site. We applied Lambert's cosine law to correct SW_{in} and SW_{out} observations given the difference between the sloped snowpacks and level radiometers (Table II). Corrections to SW_{out} directly follow Lambert's law for diffuse shortwave radiation reflecting from the snowpack and is obtained by multiplying radiometer-measured SW_{out} ($SW_{out,meas}$) by the cosine of the slope angle (s):

$$SW_{out} = SW_{out,meas}\cos(s) \quad (5)$$

$$\cos(i) = \cos(s)\cos(A_{sun} - A_{slope}) \quad (6)$$

while corrections to SW_{in} also accounts for the aspect of the slope and position of the sun via the solar azimuth angle, which we calculated following Campbell and Norman (1998).

RESULTS

We focus our study on what we call the 'common melt period' between 1 April 2012 and 16 May 2012 (day of year 92–137, noting that 2012 is a leap year), the time during which high-quality radiometric observations existed for all sites and during which all snowpacks were melting. No snow was measured by the sonic depth sensor at the clear-cut site on 16 May 2012 noting that patchy snow remained in the vicinity of the tower. The snowfall event on 27 and 28 May, after the clear-cut site had fully melted, is excluded from the analysis. The beginning of the common melt period coincides with the day at which snowpacks are commonly compared (Mote, 2003). We first describe the vegetation characteristics and microclimate of the different study sites before quantifying energy fluxes among the different snowpacks including subcanopy measurements of λE and H measurements from the lodgepole pine site. We focus our analysis on the cumulative sums of energy flux terms during the common melt period.

Stand characteristics

Average diameter at breast height was lowest at the mixed stand, reflecting a large contribution of smaller trees, and basal area was lowest at the subcanopy stand (Table II). The MPB-infested site had the highest basal area and also the highest level of MPB-induced mortality (53%). Mean stand height was similar between the MPB-infested site (20 m) and the mixed site (22 m), and the lodgepole pine forest was slightly shorter at 16 m.

Snow depth

The ablation period – approximated as the point at which snow depth first declined – began at all sites on or around 20 March 2012 (Figure 2) following a snowfall event shortly after the snowpacks reached an isothermal state (e.g. 19 March at the MPB-infested site; Figure 3). Two notable snowfall events occurred on 7 and 28–29 April (Figures 2 and 3). Snow depth at the beginning of

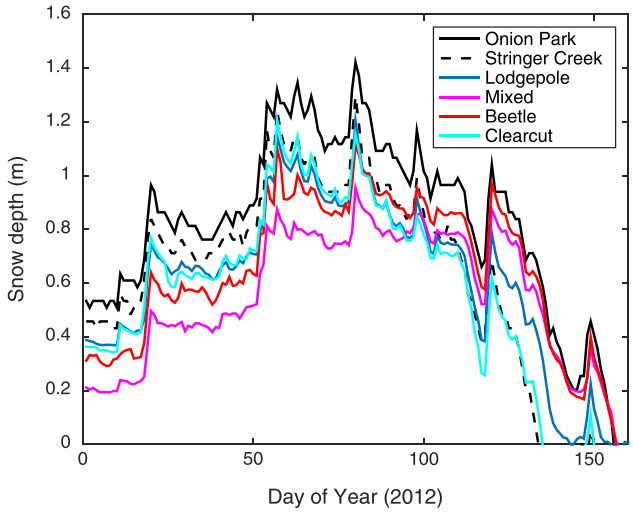


Figure 2. Daily minimum snow depth measured at the Onion Park and Stringer Creek SNOwpack TELemetry sites and the lodgepole pine, mixed forest site, beetle-infested, and clear-cut study sites in the Tenderfoot Creek Experimental Forest, Montana, during 2012

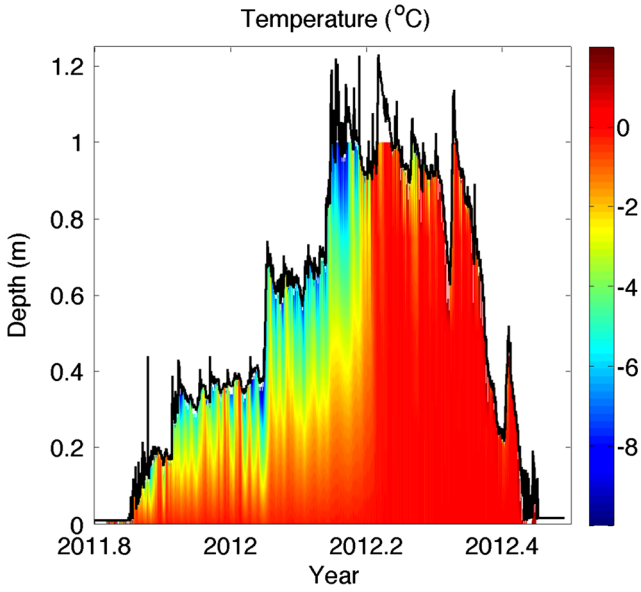


Figure 3. Interpolated half-hourly snow temperature at the mountain pine beetle-infested site at the Tenderfoot Creek Experimental Forest, Montana, from observations of air temperature at the adjacent mixed coniferous site and a snow temperature ladder. The snowpack became isothermal on 24 March 2012

the ablation period was 1.20 m at the lodgepole pine site, 1.16 m at the clear-cut site, and 1.12 m at the MPB-infested site, but only 0.95 m at the mixed coniferous site. Snow depth was still 0.43 m at both the MPB-infested and mixed coniferous sites and 0.22 m at the lodgepole pine site when the clear-cut site had fully melted on 16 May 2012. The mean snow depth depletion rate during the common melt period and during days in which snow depth was decreasing was $-0.036\,\mathrm{m\,day^{-1}}$ at the lodgepole pine site, $-0.029\,\mathrm{m\,day^{-1}}$ at the MPB-infested site, $-0.024\,\mathrm{m\,day^{-1}}$ at the mixed coniferous site, and $-0.039\,\mathrm{m\,day^{-1}}$ at the clear-cut site.

Snow water equivalent model and energy balance closure

A linear model of SWE (SWE_s) based on observations from Onion II explained 96% of the variability of manual SWE measurements from the lodgepole pine site and had the lowest Akaike information criterion and Bayesian information criterion values of any model tested (Figure 4). For analyses of energy balance closure at the lodgepole pine site we, subsequently use the following model:

$$\mathrm{SWE_s} = 1.4 \times \text{Onion II} - 0.0076 \text{ m} \qquad (7)$$

Energy balance closure, approximated as the sum of R_{net}, G, λE, and H *versus* $Q_{m,m}$, exceeded 80% during times early in the melt period and averaged 69% across the entire common melt period (Figure 5).

Air, snow, and soil temperature

Mean T_a during the common melt period was 1.5 °C at the lodgepole pine site, 0.9 °C at the mixed site (noting that the MPB-infested site was within 15 m), and 2.2 °C at the clear-cut site. T_{soil} was frequently less than 0 °C at the lodgepole pine site during the common melt period but was approximately 0 °C during most of the common melt period at the clear-cut site (Figure 6). We can apply the Stephen–Boltzmann law to test the assumption that T_{ss} was approximately 0 °C throughout the common melt period:

$$LW_{out} = A\varepsilon_{ss}\sigma T_{ss}^4 \qquad (8)$$

where A is a view factor assumed to be one for flat surfaces, ε_{ss} is the emissivity of the snow surface generally

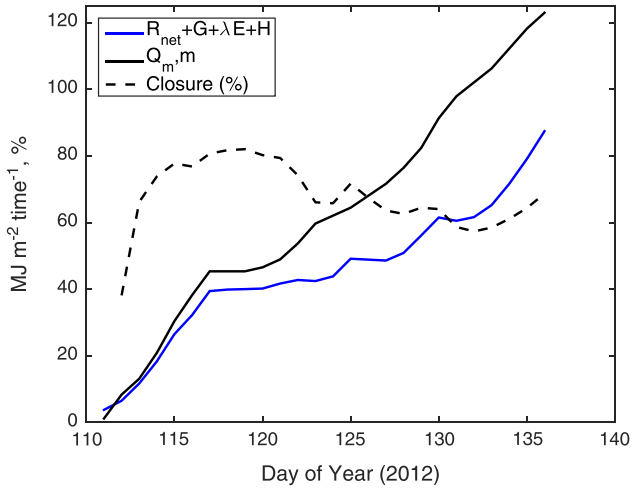


Figure 5. The cumulative sum of daily energy inputs and outputs to snow (Equation (1)) via net radiation (R_{net}), soil heat flux (G), latent heat flux (λE), and sensible heat flux (H) compared with modelled energy required for snowmelt (Q_m,m) from Equation (4). The time course of energy balance closure – the ratio of measured energy flux and modelled energy required for snowmelt – is presented as a dashed line

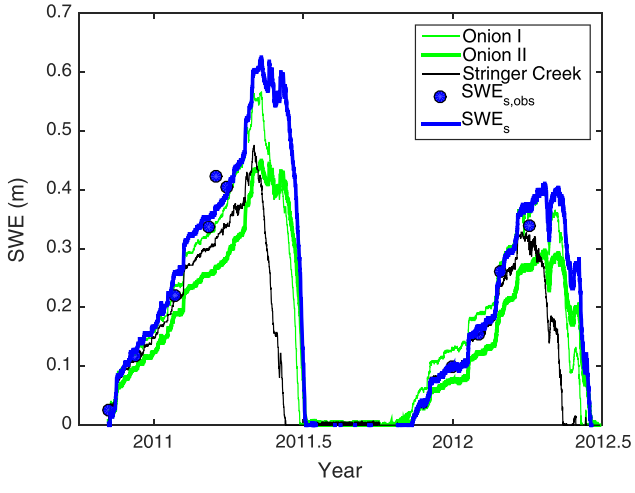


Figure 4. Snow water equivalent (SWE) from the Onion Park and Stringer Creek SNOwpack TELemetry sites in the Tenderfoot Creek Experimental Forest, with manual SWE observations from the lodgepole pine study site ($SWE_{s,obs}$) and modelled SWE ($\mathrm{SWE_s}$) following Equation (7)

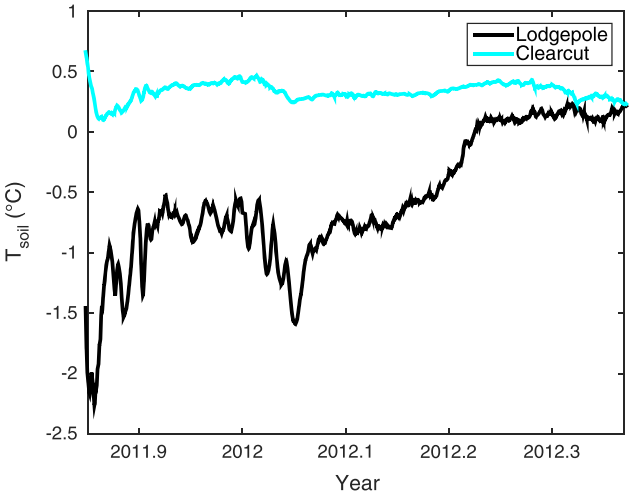


Figure 6. Soil temperature (T_{soil}) measured at 5-cm depth at the lodgepole pine and clear-cut study sites during the snow-covered period of the 2012 water year

considered to be 0.97 (Hardy *et al.*, 1997), and σ is the Stefan–Boltzmann constant (5.67×10^{-8} W m^{-2} K^{-4}). The cumulative sum of LW_{out} for the common melt period assuming $T_{ss} = 273.15$ K is 1190 MJ m^{-2} 45 days^{-1}, which differed by less than 0.8% from the cumulative sum of measured LW_{out} at all of the study sites (1190–1200 MJ m^{-2} 45 days^{-1}).

Shortwave radiation

The cumulative sum of SW_{in} for the common melt period was 275 MJ m^{-2} 45 days^{-1} at the lodgepole pine site, 195 MJ m^{-2} 45 days^{-1} at the MPB-infested site, 145 MJ m^{-2} 45 days^{-1} at the mixed coniferous site, and 865 MJ m^{-2} 45 days^{-1} at the clear-cut site (Figure 7A). In other words, the lodgepole pine, MPB-infested, and mixed coniferous sites received 32%, 23%, and 17% of the shortwave radiation incident on the clear-cut site, respectively, during the common melt period. These differences reflected a calculated *PAI* of 4.1 (m^2 m^{-2}) at the lodgepole pine site, 5.3 at the MPB-infested site, and 5.5 at the mixed coniferous site (Table II).

The cumulative sum of SW_{out} was 165 MJ m^{-2} 45 days^{-1} at the lodgepole pine site, 120 MJ m^{-2} 45 days^{-1} at the MPB-infested site, 85 MJ m^{-2} 45 days^{-1} at the mixed coniferous site, and 560 MJ m^{-2} 45 days^{-1} at the clear-cut site (Figure 7B); the snowpack of the lodgepole pine site reflected approximately as much shortwave radiation as the MPB-infested and mixed coniferous snowpacks received. SW_{net} was 110 MJ m^{-2} 45 days^{-1} at the lodgepole pine site, 75 MJ m^{-2} 45 days^{-1} at the MPB-infested site, 60 MJ m^{-2} 45 days^{-1} at the mixed coniferous site, and 300 MJ m^{-2} 45 days^{-1} at the clear-cut site (Figure 7C).

Albedo

An integrated albedo,

$$\sum SW_{out} / \sum SW_{in} \tag{9}$$

for the common melt period was calculated to be 0.60 for the lodgepole pine site, 0.62 for the MPB-infested site, 0.59 for the mixed coniferous site, and 0.65 at the clear-cut site. Embedded within these integrated albedo values for the common melt period are distinct temporal differences in albedo calculated using daily sums of shortwave energy flux (Figure 8). The lodgepole pine site had a high albedo value of ~0.8 until the rapid snowmelt period during the week of 20 April 2012 (Figures 2 and 3) after which it reached ~0.5, then returned to above 0.7 for over a week after the snowfall event of 28–29 April until the rapid melt period that began around 8 May. Other snowpacks followed similar patterns except

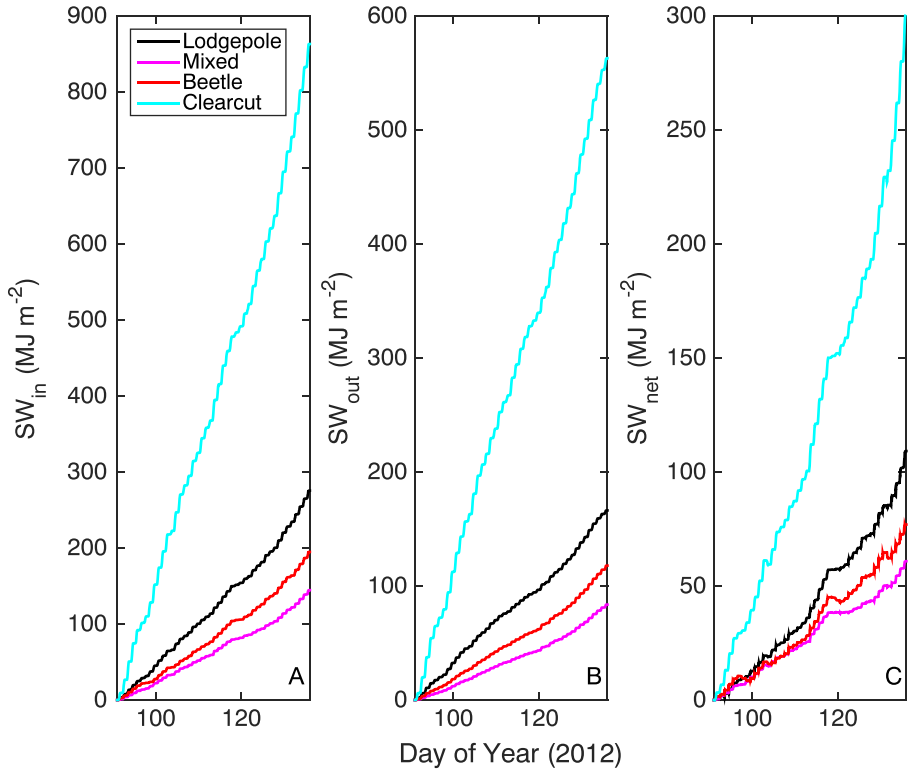


Figure 7. Incident (SW_{in}, A), outgoing (SW_{out}, B), and net (SW_{net}, C) shortwave radiation flux at the lodgepole pine ('Lodgepole'), mixed coniferous ('Mixed'), mountain pine beetle-infested ('Beetle'), and clear-cut study sites during the 2012 study period at the Tenderfoot Creek Experimental Forest, Montana

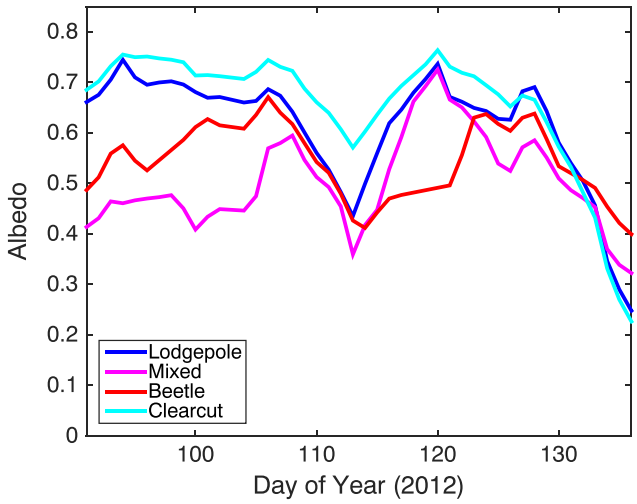


Figure 8. Daily shortwave albedo, calculated using Equation (9), for snowpacks in lodgepole pine ('Lodgepole'), mixed coniferous ('Mixed'), mountain pine beetle-infested ('Beetle'), and clear-cut study site snowpacks during the 2012 study period, displayed as the output of a seven-day digital filter

albedo at the mixed coniferous site was only ~0.5 until the 28–29 April snow event and albedo at the clear-cut site only decreased to ~0.6 immediately before the 28–29 April snow event.

Longwave radiation

LW_{out} during the common melt period among the study sites differed by <1% as noted. The cumulative sum of LW_{in} during the common melt period was 1190 MJ m^{-2} 45 days^{-1} at the lodgepole site, 1200 MJ m^{-2} 45 days^{-1} at the MPB-infested site, 1210 MJ m^{-2} 45 days^{-1} at the mixed coniferous stand, and 1020 MJ m^{-2} 45 days^{-1} at the clear-cut site (Figure 9A). As a consequence, the cumulative sum of LW_{net} was −9 MJ m^{-2} 45 days^{-1} at the lodgepole site, 3 MJ m^{-2} 45 days^{-1} at the MPB-infested site, 18 MJ m^{-2} 45 days^{-1} at the mixed coniferous stand, and −170 MJ m^{-2} 45 days^{-1} at the clear-cut site (Figure 9B). In other words, the snowpacks of the lodgepole pine and clear-cut sites lost thermal energy to the atmosphere during the common melt period and the MPB-infested and mixed coniferous snowpacks gained thermal energy from above.

Net radiation

The cumulative sum of R_{net} (Equation (2)) during the common melt period was 100 MJ m^{-2} 45 days^{-1} at the lodgepole site, 79 MJ m^{-2} 45 days^{-1} at the MPB-infested site, 77 MJ m^{-2} 45 days^{-1} at the mixed coniferous stand, and 130 MJ m^{-2} 45 days^{-1} at the clear-cut site (Figure 10). Cumulative R_{net} at the clear-cut site was only some 40% greater than the mixed coniferous site despite incident shortwave radiation flux that was nearly sixfold greater (Figure 7) because of the low albedo of the mixed coniferous snow and large losses of longwave energy from the clear-cut snowpack (Figure 9). Cumulative R_{net} at the lodgepole pine site was only some 20% greater than at the MPB-infested site despite nearly 50% greater SW_{net} because in part of a 13 MJ m^{-2} 45 days^{-1} difference in LW_{net} (Figures 9 and 10). Mechanisms underlying these similarities and differences in cumulative R_{net} are further described in the Discussion section.

Sensible, latent, and ground heat flux and total energy available for snowmelt

Energy inputs into the snowpack at the lodgepole site via H (22 MJ m^{-2} 45 days^{-1}) approximately equalled losses via λE (−25 MJ m^{-2} 45 days^{-1}, Figure 11). G at the lodgepole pine site represented a trivial component of Q_m at only 0.3 MJ m^{-2} 45 days^{-1} (and −6 MJ m^{-2} 45 days^{-1} at the clear-cut site). Assuming the frequently used value of 3.13 W m^{-2} would have resulted in a 12 MJ m^{-2} overestimate of G over the common melt period, similar in magnitude to the sum of LW_{net} at the lodgepole pine site. As a consequence of these turbulent, conductive, and radiative energy fluxes (Equation (1)), the cumulative sum of Q_m at the lodgepole pine site during the common melt period was 97 MJ m^{-2} 45 days^{-1}.

DISCUSSION

The objectives of this study were to improve understanding of the early stages of MPB infestation on snow ablation and to quantify how energy inputs into mountain snowpacks change across a space-for-time succession and management chronosequence of healthy, MPB-infested, mixed coniferous, and clear-cut snowpacks; forests in the grey-stage of MPB disturbance were rare during the measurement period (Kaiser *et al.*, 2012). We first discuss eddy covariance energy balance closure and energy fluxes, followed by simple simulations of snow energy inputs under different canopy and snow surface conditions. We finish with a prospectus for future snow research in MPB-impacted forests, many of which are currently undergoing management and successional trajectories following the peak in new MPB-infested area in 2009 (Man, 2012).

Energy balance closure and eddy covariance measurements

The estimated eddy covariance energy balance closure of ~70% (Figure 5) is lower than the FLUXNET network of eddy covariance research sites, 73% (Stoy *et al.*, 2013), noting that the FLUXNET towers are above forest canopies where one may expect turbulence

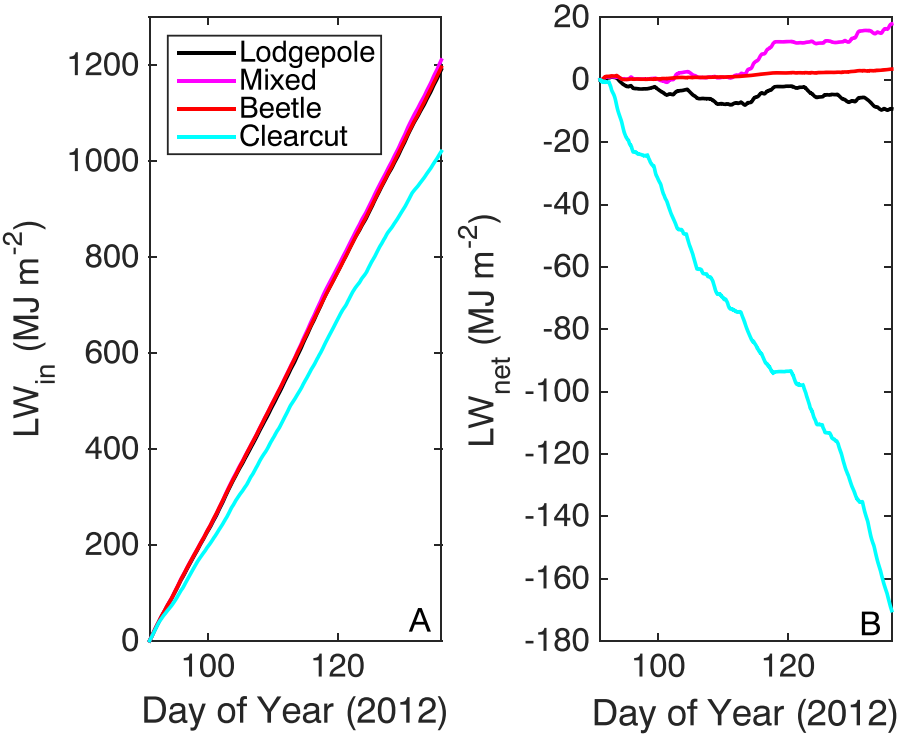


Figure 9. Incident (LW_{in}, A) and net (LW_{net}, B) longwave radiation flux at the lodgepole pine ('Lodgepole'), mixed coniferous ('Mixed'), mountain pine beetle-infested ('Beetle'), and clear-cut study sites during the 2012 study period at the Tenderfoot Creek Experimental Forest, Montana

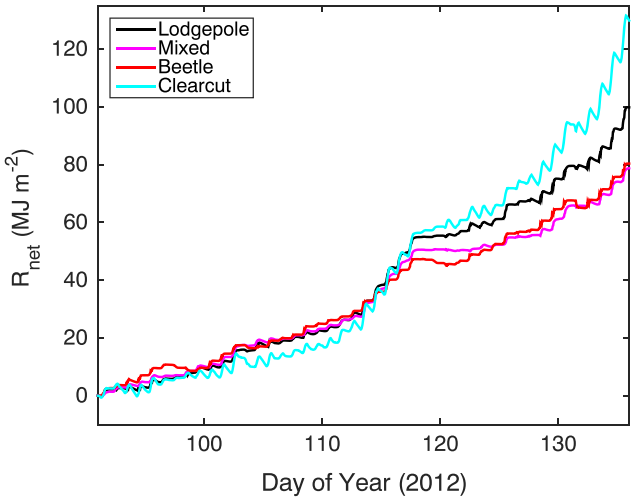


Figure 10. Net radiation flux (R_{net}) at the lodgepole pine ('Lodgepole'), mixed coniferous ('Mixed'), mountain pine beetle-infested ('Beetle'), and clear-cut study sites during the 2012 study period at the Tenderfoot Creek Experimental Forest, Montana

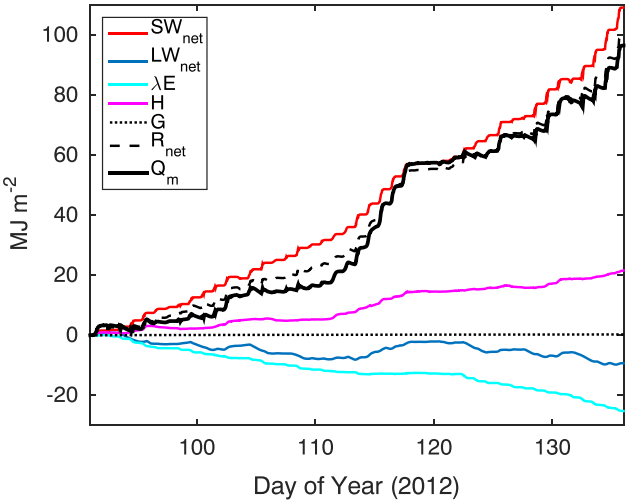


Figure 11. The cumulative sum of net shortwave radiation (SW_{net}), net longwave radiation (LW_{net}), evapotranspiration (λE), sensible heat flux (H), soil heat flux (G), net radiation (R_{net}), and available energy for snowmelt (Q_m) in a lodgepole pine forest in the Tenderfoot Creek Experimental Forest during the 2012 study period

to be better-developed. Studies of the eddy covariance energy balance often apply the approach of Twine *et al.* (2000) in which a Bowen ratio (β)-based correction is applied to H and λE to force the energy balance to become closed ($\beta = H/LE$). We lack information on half-hourly energy balance closure to apply the approach of Twine *et al.* (2000) in the typical manner because the model for $Q_{m,m}$ (Equation (4)) is based on dSWE, which can change by a minimum of 0.254 cm (0.1 in.) owing to the sensitivity of the SNOTEL instrumentation.

This amount of SWE requires 110 W m^{-2} of energy to melt, and observed R_{net} at the lodgepole pine site was greater than 110 W m^{-2} during only 7% of the available half-hours during the measurement period. In other words, the smallest possible change in $Q_{m,m}$ is larger than the net amount of radiative energy under most conditions. Applying a correction to H and λE based on $Q_{m,m}$ would therefore frequently misrepresent energy balance closure on a half-hourly basis. If we apply the approach of Twine *et al.* (2000) to the entire period displayed in Figure 5, the values of β for which $R_{net}+G+\beta\lambda E+H/\beta$ equals $Q_{m,m}$ over the common melt period, 122 MJ m^{-2} 45 days^{-1}, is either -1.48 or 0.60. Correction using the former results in a cumulative sum of λE of ~37 MJ m^{-2} 45 days^{-1} and H of -15 MJ m^{-2} 45 days^{-1}, which are opposite signs of what is observed. Correction using the latter results in a cumulative sum of λE of -15 MJ m^{-2} 45 days^{-1} and H of 37 MJ m^{-2} 45 days^{-1}, which is plausible for λE but the cumulative sum of H is two-thirds that of R_n, which likewise seems implausible. The challenge for adopting a correction is that H and λE are of opposing sign on average during the common melt period, and it is unclear how to correct our observations to close the energy balance if such a correction is needed (Baldocchi, 2008). Regardless, the magnitude of subcanopy H and λE measured here is somewhat larger than previous models, suggesting that the contribution of H and λE to snowmelt under forested canopies requires further study. Boon (2009), for example, modelled H and λE to be near zero in a living lodgepole pine stand and between 0.2 MJ m^{-2} day^{-1} (H) and -0.4 MJ m^{-2} day^{-1} (λE) in a grey-phase stand during the melt period. Our eddy covariance measured H averaged 0.5 MJ m^{-2} day^{-1} and λE averaged -0.6 MJ m^{-2} day^{-1} in the lodgepole pine stand during the common melt period.

Conditions under which sensible and latent heat fluxes are in balance

As noted, the magnitudes of energy gain to snow via H and energy loss via λE were similar in the lodgepole pine forest during the common melt period (Figure 11), and we can quantify the conditions under which the sum of H and λE is zero. The Fourier law expression for H, following the convention that heat flux into the snowpack is positive, is

$$H = \frac{\rho C_p}{r_H}(T_a - T_{ss}) \tag{10}$$

where ρ and C_p are the density and specific heat of air, respectively, T_{ss} is assumed to be 0 °C for melting snow, and r_H is the resistance of the surface to sensible heat flux.

The Fick law expression for λE, again under the condition that a flux of heat into the snowpack is positive, is

$$LE = \frac{\rho C_p}{\gamma^* r_H}(e_a - e[T_{ss}]) \tag{11}$$

where e_a is the atmospheric vapour pressure, $e[T_{ss}]$ is the vapour pressure at the snow surface, which we can assume to be saturated at 0 °C such that $e[T_{ss}] = 0.611$ kPa, and γ^* is the psychometric constant (γ) adjusted for the ratio between resistance to latent heat flux (r_v) and r_H. r_v is commonly considered to equal *rH in the absence of plant stomata* (Campbell and Norman, 1998) such that:

$$\gamma T_a + e_a = 0.611 \text{ kPa} \tag{12}$$

The value of e_a as a function of T_a that satisfies this equality (for $\gamma = 0.0665$ kPa°C given the elevation and therefore average atmospheric pressure of the study site) and the relative humidity that corresponds to these values of e_a, are shown in Figure 13. As noted, the average T_a and e_a during the common melt period are below the line at which H and λE are equal such that $H < -\lambda E$ (Figure 12), which is what we observe (Figure 11). Interestingly, T_a and e_a at all study sites followed the line at which H and LE are of equal and opposite sign, lending support to the idea that R_n measurements approximated Q_m (i.e. that the energy balance of snowmelt could be approximated by radiometric terms) at all sites (Figure 11).

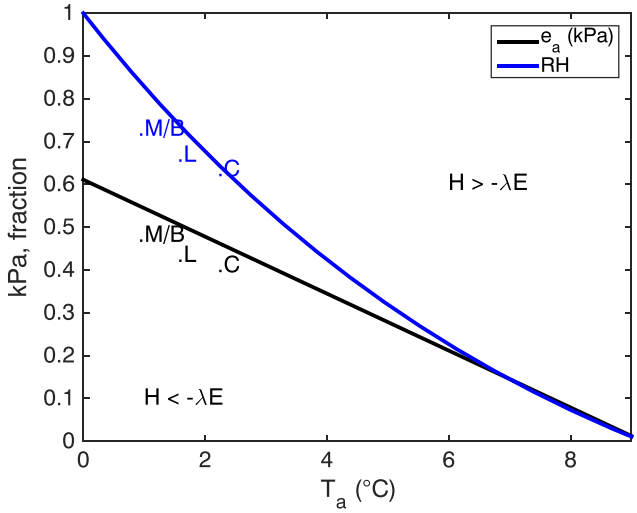


Figure 12. The value of atmospheric vapour pressure (e_a) and relative humidity (RH) as a function of air temperature (T_a) at which snowpack energy inputs from sensible heat (H) and outputs from latent heat (λE) are equal (i.e. $H = -\lambda E$). The mean values of T_a, e_a, and RH during the study snowmelt period for the lodgepole pine ('L'), adjacent mixed forest, mountain pine beetle-damaged forest ('M/B'), and clear-cut sites ('C') are plotted for reference

Shortwave radiation and albedo

Half-hourly snow albedo measurements are highly variable because of complex canopy shade effects on the upward-facing pyranometer and the snow. Regardless, the mixed coniferous forest snowpack had considerably lower albedo than the other study sites, although it is unclear if the diverse overstory had anything to do with this effect. Rather, observations are likely due to complex patterns of needlefall, which in MPB-impacted forests do not appear to be a function of wind speed over much of the wind speed range (Winkler *et al*., 2014). Mechanistic understanding of needlefall across coniferous species must be improved to improve understanding of the temporal and spatial patterns of snowmelt in North American montane forests.

Longwave radiation

Outgoing longwave radiation flux measurements confirmed that the temperature of the snow surface during the common melt period was not different from 0 °C within the limits of sensor accuracy, as expected. The sum of LW_{net} was lowest at the clear-cut site and lower at the lodgepole pine site than the other forested ecosystems, consistent with the lower PAI of these sites (Table II). The sum of LW_{net} at the MPB-infested site, however, was lower than the mixed coniferous site despite a similar PAI ($5.3\,m^2\,m^{-2}$ at the MPB-infested site and $5.5\,m^2\,m^{-2}$ at the mixed coniferous site). Observations are consistent with the notion that the desiccated needles of the MPB-infested site were less effective at insulating the subcanopy snowpack, but detailed canopy temperature measurements must be made to ascertain the degree, if any, of this effect. We note that photosynthetic activity in mountain conifers often commences as the snowpack becomes isothermal (Monson *et al*., 2005), and the needles of living trees can be assumed to be hydrated as a consequence.

If we simulate the time it takes for Q_m to reach $96\,MJ\,m^{-2}$ by replacing LW_{up} at the lodgepole pine site with observations from the other forested ecosystems in the energy balance equations (Equations (1) and (2)), the snowpack would have melted about a day faster with the denser but largely dead MPB-infested canopy, but 3 days faster (42 days) with the denser and green mixed coniferous canopy, all else being equal. In other words, increasing snowmelt rate via lower albedo in the MPB-impacted canopy is only partly offset by the dead canopy's decrease in incident longwave radiation; replacing the lodgepole pine albedo with observed albedo from the MPB-damaged or mixed canopies would have resulted in a snowpack that reached a Q_m of $96\,W\,m^{-2}$ 4 days earlier.

It should also be noted that over the common melt period, the change in PAI from 4.1 at the lodgepole pine site to 5.5 at the mixed coniferous site was enough to change the sum of LW_{net} during the common melt period from $-10\,MJ\,m^{-2}\,45\,days^{-1}$ to $+18\,MJ\,m^{-2}\,45\,days^{-1}$, noting also that T_a at the north-facing mixed coniferous site was ~0.5 °C cooler. Results suggest that changes in stand density that are characteristic of coniferous forests in the Rocky Mountain region (Spanner *et al*., 1990) may change LW_{net} during the melt period from a net output to a net input.

The effects of snow on radiometric measurements

Snowfall during the snowmelt period intermittently impeded incident shortwave and longwave radiation from reaching the radiometers, especially in the less-windy subcanopy environments. Ascertaining the precise periods when snow covers a radiometer in the complex light environment beneath a forest canopy can be difficult because both snow and trees impede direct radiation. We assumed that radiometers were blocked when the daily sum of shortwave radiation exceeded the daily sum of incident radiation. These periods tended to follow snowfall events during the melt period (Figures 2 and 3). SW_{in} observations at the forest sites for these periods were replaced by SW_{in} observations from the windier clear-cut site scaled by the ratio of SW_{in} between forest and clear-cut sites during the days where the subcanopy radiometers were not impeded.

Soil heat flux

Differences in soil heat flux among the lodgepole pine and clear-cut sites during the common melt period reflected the antecedent temperature conditions of the soil (Figure 6). T_{soil} at lodgepole pine site was less than −0.5 °C for much of the snow-covered period and received $0.3\,MJ\,m^{-2}$ of energy from the snowpack during the common melt period. The soil at the clear-cut site, however, contributed $6\,MJ\,m^{-2}$ to the snowpack during the common melt period because temperatures averaged slightly above zero during the snow-covered period. These differences can be understood in terms of the heat flux received by the lodgepole pine and clear-cut soils during the preceding non-snow-covered season (Figure 13). Snow melted some 10 days earlier at the clear-cut site in 2011, and maximum cumulative non-snow-covered season G was nearly 30% greater at the clear-cut site (~$90\,MJ\,m^{-2}$) than at the lodgepole pine site (~$70\,MJ\,m^{-2}$), resulting in warmer T_{soil} during the beginning of the snow-covered period (Figure 6). If the annual sum of G is to approximate zero under steady-state conditions, more soil heat must be lost from the clear-cut site than the lodgepole pine site during the snow-covered period.

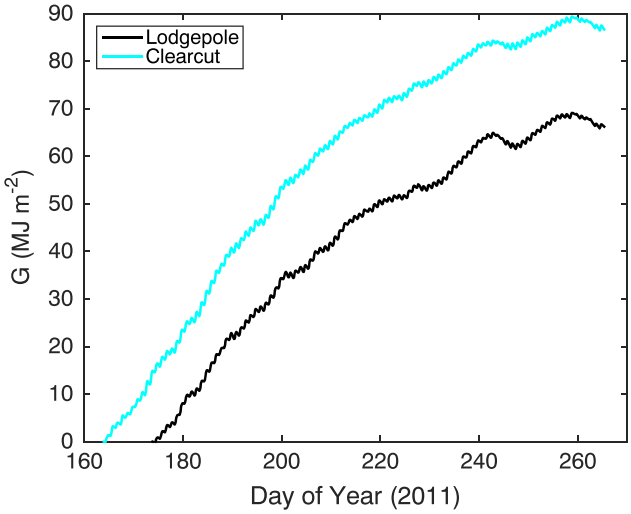


Figure 13. Soil heat flux (G) in the lodgepole pine forest and clear-cut study ecosystems during summer (2011), before the 2012 study period

Future work

Our study highlights a number of uncertainties that require future study. The possibility that (desiccated) red needles absorb and re-emit less longwave radiation may be a mechanism by which longwave energy loss from the snowpack is discouraged, resulting in longer snow duration than may otherwise be expected. Eddy covariance measurements demonstrated that the contributions of H and λE were approximately in balance because atmospheric temperature and moisture conditions during the common melt period were near the relationship with which these two terms are in balance (Figure 12), but additional work must understand the consequences of lack of energy balance closure on the magnitude of these fluxes. Importantly, understory and non-dominant species play an important role in snowmelt (Winkler *et al*., 2014), especially as more plant material becomes exposed from a melting snowpack. Subcanopy structure is difficult to ascertain from remote platforms but is an important factor for current year snowmelt and future snowmelt if these individuals eventually come to dominate the overstory. Reactive management (i.e. harvesting), mixed stands (Stone and Wolfe, 1996), lodgepole-dominated stands, and/or changes to fire activity may follow MPB disturbance. Whereas MPB outbreak severity is largely unrelated to fire severity (Harvey *et al*., 2014), green attack and red-stage canopies tend to experience more severe fires under moderate burning conditions (Harvey *et al*., 2014). Combined with other studies, our results suggest that the future of snowmelt in MPB-impacted forests needs to consider management response and community succession along the characteristic time scales of post-MPB forest recovery of decades or longer (Vanderhoof and Williams, 2015).

ACKNOWLEDGEMENTS

We would like to thank the Montana Water Center, the State of Montana, and the Montana State University Center for Faculty Excellence for financial support; Dr Lucy Marshall and Elizabeth S. K. Harris for constructive comments on the manuscript; and Fabian Nippgen, Kelsey Jencso, and Paddy Stoy for advice and support in the field. Eddy covariance and meteorological observations in support of this manuscript are archived by Ameriflux.

AUTHOR CONTRIBUTIONS

C. M. W. and P. C. S. designed the experiment with input from B. L. M. C. M. W., P. C. S., F. A. R., A. V. J., and B. L. M. performed fieldwork with field assistance as noted in the Acknowledgements. C. M. W., P. C. S., and F. A. R. analysed the data, and F. A. R. processed the eddy covariance data. A. V. J. created Figure 1; C. M. W., F. A. R., and P. C. S. organized the data and assisted in submitting the data to public repositories; and B. L. M. contributed to logistics. All authors contributed to writing the manuscript.

REFERENCES

Aukema BH, Carroll AL, Zheng Y, Zhu J, Raffa KF, Dan Moore R, Stahl K, Taylor SW. 2008. Movement of outbreak populations of mountain pine beetle: influences of spatiotemporal patterns and climate. *Ecography (Cop.)* **31**(3): 348–358. DOI:10.1111/j.2007.0906-7590.05453.x.

Baldocchi DD. 2008. "Breathing" of the terrestrial biosphere: lessons learned from a global network of carbon dioxide flux measurements systems, Turner Review. *Australian Journal of Botany* **56**: 1–26.

Barnett TP, Adam JC, Lettenmaier DP. 2005. Potential impacts of a warming climate on water availability in snow-dominated regions. *Nature* **438**(7066): 303–309. DOI:10.1038/nature04141.

Bearup LA, Maxwell RM, Clow DW, McCray JE. 2014. Hydrological effects of forest transpiration loss in bark beetle-impacted watersheds. *Nature Climate Change* **4**(6): 481–486.

Biederman JA, Brooks PD, Harpold AA, Gochis DJ, Gutmann E, Reed DE, Pendall E, Ewers BE. 2014. Multiscale observations of snow accumulation and peak snowpack following widespread, insect-induced lodgepole pine mortality. *Ecohydrology* **7**(1): 150–162. DOI:10.1002/eco.1342.

Boon S. 2009. Snow ablation energy balance in a dead forest stand. *Hydrological Processes* . DOI:10.1002/hyp.

Burles K, Boon S. 2011. Snowmelt energy balance in a burned forest plot, Crowsnest Pass, Alberta, Canada. *Hydrological Processes* **25**(19): 3012–3029.

Campbell GS, Norman JM. 1998. *An Introduction to Environmental Biophysics*, 2nd edition. Springer: New York.

Cayan DR. 1996. Interannual climate variability and snowpack in the western United States. *Journal of Climate* **9**(5): 928–948.

Dominguez F, Rivera E, Lettenmaier DP, Castro CL. 2012. Changes in winter precipitation extremes for the western United States under a warmer climate as simulated by regional climate models. *Geophysical Research Letters* **39**(5): 1–7. DOI:10.1029/2011GL050762.

Emanuel RE, Epstein HE, McGlynn BL, Welsch DL, Muth DJ, D'Odorico P. 2010. Spatial and temporal controls on watershed ecohydrology in the northern Rocky Mountains. *Water Resources Research* **46**(11): 1–14. DOI:10.1029/2009WR008890.

Emanuel RE, Riveros-Iregui DA, McGlynn BL, Epstein HE. 2011. On the spatial heterogeneity of net ecosystem productivity in complex landscapes. *Ecosphere* **2**(7): art86. DOI:10.1890/ES11-00074.1.

Falge E, Baldocchi DD, Olson R, Anthoni P, Aubinet M, Bernhofer C, Burba G, Ceulemans R, Clement R, Dolman H, Granier A, Gross P, Grünwald T, Hollinger D, Jensen NO, Katul GG, Keronen P, Kowalski A, Lai CT, Law BE, Meyers T, Moncrieff J, Moors E, Munger JW, Pilegaard K, Rannik Ü, Rebmann C, Suyker A, Tenhunen J, Tu K, Verma S, Vesala T, Wilson K, Wofsy S. 2001. Gap filling strategies for long term energy flux data sets. *Agricultural and Forest Meteorology* **107**: 71–77. DOI:10.1016/S0168-1923(00)00235-5.

Farnes PE, Shearer RC, McCaughey WW, Hanson KJ. 1995. Comparisons of hydrology, geology, and physical characteristics between tenderfoot creek experimental forest (east side) Montana, and Coram experimental forest (west side) Montana.

Hamlet AF, Mote PW, Clark MP, Lettenmaier DP. 2007. Twentieth-century trends in run-off, evapotranspiration, and soil moisture in the western United States. *Journal of Climate* **20**(8): 1468–1486. DOI:10.1175/JCLI4051.1.

Hardy JP, Davis RE, Jordan R, Li X, Woodcock C, Ni W. 1997. Snow ablation modeling at the stand scale in a boreal jack pine forest. *Journal of Geophysical Research* **102**(96): 397–405.

Harestad AS, Bunnell FL. 1981. Prediction of snow-water equivalents in coniferous forests. *Canadian Journal of Forest Research* **11**(4): 854–857.

Harvey BJ, Donato DC, Romme WH, Turner MG. 2014. Fire severity and tree regeneration following bark beetle outbreaks: the role of outbreak stage and burning conditions. *Ecological Applications* **24**: 1608–1625. DOI:10.1890/13-1851.1.

Harvey BJ, Donato DC, Turner MG. 2014. Recent mountain pine beetle outbreaks, wildfire severity, and postfire tree regeneration in the US Northern Rockies. *Proceedings of the National Academy of Sciences* **111**: 15120–15125. DOI:10.1073/pnas.1411346111.

Jencso KG, McGlynn BL. 2011. Hierarchical controls on run-off generation: topographically driven hydrologic connectivity, geology, and vegetation. *Water Resources Research* **47**(11): 1–16. DOI:10.1029/2011WR010666.

Jessie E, Carroll AL, Taylor SW. 2003. Effect of climate change on range expansion by the mountain pine beetle in British Columbia.

Kaiser KE, McGlynn BL, Emanuel RE. 2012. Ecohydrology of an outbreak: mountain pine beetle impacts trees in drier landscape positions first. *Ecohydrology* **6**(3): 444–454. DOI:10.1002/eco.1286.

Kurz WA, Dymond CC, Stinson G, Rampley GJ, Neilson ET, Carroll AL, Ebata T, Safranyik L. 2008. Mountain pine beetle and forest carbon feedback to climate change. *Nature* **452**(7190): 987–990. DOI:10.1038/nature06777.

Leuning R, van Gorsel E, Massman WJ, Isaac PR. 2012. Reflections on the surface energy imbalance problem. *Agricultural and Forest Meteorology* **156**: 65–74. DOI:10.1016/j.agrformet.2011.12.002.

Logan JA, Powell JA. 2001. Ghost forests, global warming, and the mountain pine beetle (Coleoptera: Scolytidae). *American Entomologist* **47**(3): 106–173.

Luo YQ, Medlyn BE, Hui DF, Ellsworth D, Reynolds J, Katul GG. 2001. Gross primary productivity in Duke Forest: modeling synthesis of CO_2 experiment and eddy-flux data. *Ecological Applications* **11**: 239–252.

Lynch HJ, Renkin RA, Crabtree RL, Moorcroft PR. 2006. The influence of previous mountain pine beetle (*Dendroctonus ponderosae*) activity on the 1988 Yellowstone fires. *Ecosystems* **9**(8): 1318–1327.

Maidment DR. 1992. *Handbook of Hydrology*. McGraw-Hill Inc: New York, NY, USA.

Man G. 2012. Major forest insect and disease conditions in the United States: 2011. Washington, DC.

Marks D, Dozier J. 1992. Climate and energy exchange at the snow surface in the alpine region of the Sierra Nevada 2. Snow cover energy balance. *Water Resources Research* **28**(11): 3043–3054.

Mikkelson KM, Bearup LA, Maxwell RM, Stednick JD, McCray JE, Sharp JO. 2013. Bark beetle infestation impacts on nutrient cycling, water quality and interdependent hydrological effects. *Biogeochemistry* **115**(1–3): 1–21. DOI:10.1007/s10533-013-9875-8.

Mincemoyer SA, Birdsall JL. 2006. Vascular flora of the tenderfoot creek experimental forest, little belt mountains, Montana. *Madrono* **53**(3): 211–222. DOI:10.3120/0024-9637(2006)53.

Misson L, Baldocchi DD, Black TA, Blanken PD, Brunet Y, Curiel Yuste J, Dorsey JR, Falk M, Granier A, Irvine MR. 2007. Partitioning forest carbon fluxes with overstory and understory eddy-covariance measurements: a synthesis based on FLUXNET data. *Agricultural and Forest Meteorology* **144**(1): 14–31.

Mitchell SR, Emanuel RE, McGlynn BL. 2015. Land–atmosphere carbon and water flux relationships to vapor pressure deficit, soil moisture, and stream flow. *Agricultural and Forest Meteorology* **208**: 108–117.

Mitton JB, Ferrenberg SM. 2012. Mountain pine beetle develops an unprecedented summer generation in response to climate warming. *American Naturalist* **179**(5): E163–E171. DOI:10.1086/665007.

Molotch N, Brooks P, Burns S, Litvak ME, Monson RK, McConnell JR, Musselman K. 2009. Ecohydrological controls on snowmelt partitioning in mixed-conifer sub-alpine forests. *Ecohydrology* **142**(May): 129–142. DOI:10.1002/eco.

Monson RK, Sparks JP, Rosenstiel TN, Scott-Denton LE, Huxman TE, Harley PC, Turnipseed AA, Burns SP, Backlund B, Hu J. 2005. Climatic influences on net ecosystem CO_2 exchange during the transition from wintertime carbon source to springtime carbon sink in a high-elevation, subalpine forest. *Oecologia* **146**(1): 130–147.

Mote PW. 2003. Trends in snow water equivalent in the Pacific Northwest and their climatic causes. *Geophysical Research Letters* **30**(12): 1601. DOI:10.1029/2003GL017258.

Nippgen F, McGlynn B, Marshall LA, Emanuel RE. 2011. Landscape structure and climate influences on hydrologic response. *Water Resources Research* **47**(12): W12528. DOI:10.1029/2011WR011161.

Pacific VJ, Jencso KG, McGlynn BL. 2010. Variable flushing mechanisms and landscape structure control stream DOC export during snowmelt in a set of nested catchments. *Biogeochemistry* **99**(1–3): 193–211. DOI:10.1007/s10533-009-9401-1.

Pacific VJ, McGlynn BL, Riveros-Iregui DA, Welsch DL, Epstein HE. 2011. Landscape structure, groundwater dynamics, and soil water content influence soil respiration across riparian–hillslope transitions in the Tenderfoot Creek Experimental Forest, Montana. *Hydrological Processes* **25**(5): 811–827.

Palmer PL. 1988. The SCS snow survey water supply forecasting program: Current operations and future directions. *Proc. West. Snow Conf. Kalispell*; 43–51.

Perrot D, Molotch NP, Musselman KN, Pugh ET. 2014. Modelling the effects of the mountain pine beetle on snowmelt in a subalpine forest. *Ecohydrology* **7**(2): 226–241. DOI:10.1002/eco.1329.

Pomeroy JW, Essery RLH. 1999. Turbulent fluxes during blowing snow: field tests of model sublimation predictions. *Hydrological Processes* **13**(18): 2963–2975.

Pomeroy JW, Gray DM, Hedstrom NR, Janowicz JR. 2002. Prediction of seasonal snow accumulation in cold climate forests. *Hydrological Processes* **16**(18): 3543–3558. DOI:10.1002/hyp.1228.

Potts D. 1984. Hydrologic impacts of a large-scale mountain pine beetle epidemic. *Water Resources Bulletin* **20**(3): 373–377.

Pugh E, Gordon E. 2013. A conceptual model of water yield effects from beetle-induced tree death in snow-dominated lodgepole pine forests. *Hydrological Processes* **27**(14): 2048–2060. DOI:10.1002/hyp.

Pugh E, Small E. 2012. The impact of pine beetle infestation on snow accumulation and melt in the headwaters of the Colorado River. *Ecohydrology* **5**(4): 467–477. DOI:10.1002/eco.239.

R Core Team. 2014. R: a language and environment for statistical computing.

Raffa KF, Aukema BH, Bentz BJ, Carroll AL, Hicke JA, Turner MG, Romme WH. 2008. Cross-scale drivers of natural disturbances prone to anthropogenic amplification: the dynamics of bark beetle eruptions. *Bioscience* **58**(6): 501.

Rains FA. 2013. Biological and physical controls of CO_2 flux through snow in a forested ecosystem. http://scholarworks.montana.edu/xmlui/handle/1/2098.

Riveros-Iregui DA, McGlynn BL. 2009. Landscape structure control on soil CO_2 efflux variability in complex terrain: scaling from point observations to watershed scale fluxes. *Journal of Geophysical Research* **114**(G2): 1–14. DOI:10.1029/2008JG000885.

Riveros-Iregui DA, McGlynn BL, Marshall LA, Welsch DL, Emanuel RE, Epstein HE. 2011. A watershed-scale assessment of a process soil CO_2 production and efflux model. *Water Resources Research* **47**: 1–12. DOI:10.1029/2010WR009941.

Riveros-Iregui DA, McGlynn BL, Emanuel RE, Epstein HE. 2012. Complex terrain leads to bidirectional responses of soil respiration to inter-annual water availability. *Global Change Biology* **18**(2): 749–756. DOI:10.1111/j.1365-2486.2011.02556.x.

Spanner MA, Pierce LL, Peterson DL, Running SW. 1990. Remote sensing of temperate coniferous forest leaf area index the influence of canopy closure, understory vegetation and background reflectance. *International Journal of Remote Sensing* **11**(1): 95–111. DOI:10.1080/01431169008955002.

Stone WE, Wolfe ML. 1996. Modelling longwave radiation to snow beneath forest canopies using hemispherical photography or linear regression. *Vegetatio* **122**(1): 1–12. DOI:10.1007/BF00052811.

Stoy PC, Katul GG, Siqueira MBS, Juang J-Y, McCarthy HR, Oishi AC, Uebelherr JM, Kim H-S, Oren R. 2006. Separating the effects of climate and vegetation on evapotranspiration along a successional chronosequence in the southeastern U.S. *Global Change Biology* **12**: 2115–2135.

Stoy PC, Mauder M, Foken T, Marcolla B, Boegh E, Ibrom A, Arain MA, Arneth A, Aurela M, Bernhofer C, Cescatti A, Dellwik E, Duce P, Gianelle D, van Gorsel E, Kiely G, Knohl A, Margolis H, McCaughey H, Merbold L, Montagnani L, Papale D, Reichstein M, Saunders M, Serrano-Ortiz P, Sottocornola M, Spano D, Vaccari F, Varlagin AA. 2013. data-driven analysis of energy balance closure across FLUXNET research sites: The role of landscape scale heterogeneity. *Agricultural and Forest Meteorology* **171**: 137–152. DOI:10.1016/j.agrformet.2012.11.004.

Twine TE, Kustas WP, Norman JM, Cook DR, Houser PR, Meyers TP, Prueger JH, Starks PJ, Wesely ML. 2000. Correcting eddy-covariance flux underestimates over a grassland. *Agricultural and Forest Meteorology* **103**(3): 279–300.

Vanderhoof MK, Williams CA. 2015. Persistence of MODIS evapotranspiration impacts from mountain pine beetle outbreaks in lodgepole pine forests, south-central Rocky Mountains. *Agricultural and Forest Meteorology* **200**(0): 78–91. DOI:10.1016/j.agrformet.2014.09.015.

Varhola A, Coops NC, Weiler M, Moore RD. 2010. Forest canopy effects on snow accumulation and ablation: an integrative review of empirical results. *Journal of Hydrology* **392**(3–4): 219–233. DOI:10.1016/j.jhydrol.2010.08.009.

Westerling AL, Hidalgo HG, Cayan DR, Swetnam TW. 2006. Warming and earlier spring increase western U.S. forest wildfire activity. *Science* **313**(5789): 940–943. DOI:10.1126/science.1128834.

Wilson K, Goldstein A, Falge E, Aubinet M, Baldocchi DD, Berbigier P, Bernhofer C, Ceulemans R, Dolman H, Field C, Grelle A, Ibrom A, Law BE, Kowalski A, Meyers T, Moncrieff J, Monson R, Oechel W, Tenhunen J, Valentini R, Verma S. 2002. Energy balance closure at FLUXNET sites. *Agricultural and Forest Meteorology* **113**: 223–243. DOI:10.1016/S0168-1923(02)00109-0.

Winkler R, Boon S, Zimonick B, Baleshta K. 2010. Assessing the effects of post-pine beetle forest litter on snow albedo. *Hydrological Processes* **24**(6): 803–812. DOI:10.1002/hyp.7648.

Winkler R, Boon S, Zimonick B, Spittlehouse D. 2014. Snow accumulation and ablation response to changes in forest structure and snow surface albedo after attack by mountain pine beetle. *Hydrological Processes* **28**(2): 197–209. DOI:10.1002/hyp.9574.

Woods SW, Ahl R, Sappington J, McCaughey W. 2006. Snow accumulation in thinned lodgepole pine stands, Montana, USA. *Forest Ecology and Management* **235**(1-3): 202–211. DOI:10.1016/j.foreco.2006.08.013.

APPENDIX A: GAPFILLING MICROMETEOROLOGICAL DATA

Few observations went missing because of the sensor error or maintenance during the common melt period, and missing data were gapfilled to obtain consecutive time series for analysis (Falge *et al.*, 2001). Air and soil temperature observations were gapfilled using linear relationships with nearby sensors. Radiometric observations were carefully screened for periods that were consistent with snow accumulation on the radiometer and corrected as described in the following.